Nanoscale

Accepted Manuscript

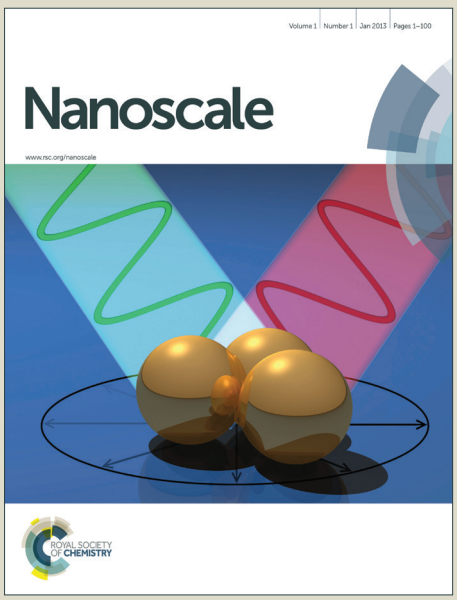

ROYAL SOCIETY OF CHEMISTRY

www.rsc.org/nanoscale

Silver Nanowires as Receiving-Radiating Nanoantennas in Plasmon-Enhanced Up-Conversion Processes

D. Piatkowski[1,2,*], N. Hartmann[1], T. Macabelli[1], M. Nyk[3], S. Mackowski[2], A. Hartschuh[1]

[1] Department Chemie and CeNS, Ludwig-Maximilians-Universität München, 81377 München, Germany

[2] Institute of Physics, Faculty of Physics, Astronomy and Informatics,
Nicolaus Copernicus University, Grudziadzka 5, 87-100 Torun, Poland

[3] Institute of Physical and Theoretical Chemistry, Wroclaw University of Technology,
Wybrzeze Wyspianskiego 27, 50-370 Wroclaw, Poland

** corresponding author: dapi@fizyka.umk.pl*

Abstract

We demonstrate efficient coupling between plasmons in a single silver nanowire and nanocrystals doped with rare earth ions, α-$NaYF_4$:Er^{3+}/Yb^{3+}. Plasmonic interaction results in a sevenfold increase of the up-converted emission of nanocrystals located in the vicinity of the nanowires as well as much faster luminescence decays. The enhancement of the emission can be precisely controlled by the polarization of the excitation laser and is significantly stronger for polarization parallel to the nanowire antennas. Imaging of angular-resolved emission patterns in the Fourier plane reveals plasmon-mediated luminescence, where the up-converted radiation is emitted via the nanowire antennas as leakage radiation.

1. Introduction

Interaction between an emitter and a metallic nanoparticle (NP) has been one of the most exciting and spectacular nanoscale effects in recent years. Surface plasmon oscillations that are localized in metallic NPs can be used to control the physical properties of luminescence emitters, particularly their absorption and emission rates,[1,2] photostability as well as efficiency of energy transfer[3,4]. Plasmon-enhanced fluorescence has been observed for various emitters such as dye molecules,[5] photosynthetic[6] or green fluorescent proteins,[7] quantum dots,[8,9] and nanocrystals doped with rare-earth ions.[10,11,12] In emitter-metal coupled systems many-fold (typically 5-20) increases of fluorescence intensity accompanied with strong shortening of the lifetimes[2] were usually observed. Enhancements strongly depend on the distance between the emitter and metallic nanoparticle, demonstrated by near-field microscopy experiments[13].

Investigations of the properties of plasmonic systems have been additionally stimulated by the diversity of available metallic nanoparticles. A wide range of protocols of synthesizing gold and silver nanoparticles with different shapes and sizes including spheres, shells, rods, wires, triangles, cubes, stars etc. has resulted in expanding available plasmon resonances from ultraviolet to near-infrared range.[14,15,16] Among

metallic nanostructures long plasmonically active nanowires are particularly interesting. They feature small diameters (~100 nm) and lengths from 1 to 10 µm and exhibit a broad plasmonic resonance profile, which in the case of silver extends from 400 nm up to 1 µm.[17] Plasmon excitations in silver nanowires can efficiently propagate and therefore transport energy for quite long distances, reaching many microns.[18] By applying fluorescence microscopy it was demonstrated, that emission from quantum dots (QDs) placed close to a silver nanowire leads to formation and propagation of surface plasmons polaritons (SPPs).[19,20] It was shown that by applying numerical aperture NA=0.7 of the excitation optics, excitation light can precisely address only the QDs, thus plasmons in silver nanowires can be launched exclusively via QD emission.[9] In this case fluorescence from the nanowire ends, observed in a wide-field microscope, demonstrates efficient energy transfer from the QD to the NW as well as energy propagation. The same study demonstrates that excitation energy can be transferred in the opposite direction, from the NW to the QDs.[9] It was also shown that the absorbance of nanowires is polarization sensitive,[21,22] which has been used for realizing logical operations on branched NWs coupled with QDs.[23] Hence, SPPs can induce additional plasmon-mediated absorption/emission channels that enhance absorption/emission rates depending on the polarization of the incident light.

In this work we present a comprehensive optical analysis of hybrid nanostructures comprising silver nanowires and nanocrystals doped with rare-earth (RE) ions. The latter are well known as up-converting (anti-Stokes) materials,[24] which due to their unique physical and optical properties,[25] have found diverse applications, for example as multi-modal bioimaging contrast agents[26,27] or as solar cells activators.[28,29] We show that the efficiency of the up-conversion process can be substantially enhanced by the plasmonic response of the NWs, in analogy to previous work focused on improving the up-conversion efficiency via plasmonic interactions with spherical nanoparticles.[11] Our analysis demonstrates that the nanowires act as receiving – emitting antennas. Upon illumination, energy is collected by the NWs and coupled to nearby NCs as evidenced by polarization-resolved luminescence imaging. Conversely, luminescence energy is partly back transferred from the NCs to the NWs and emitted by the NWs via leakage radiation. The latter was directly observed using Back Focal Plane (BFP) imaging. This new emission channel mediated by the NWs lead to an increased radiative relaxation rate which we monitored by time-resolved PL measurements. The spatial variation of the radiative rate enhancement along the nanowires was visualized using fluorescence-lifetime imaging microscopy (FLIM) revealing that most efficient enhancement of the radiative rate occurs at the nanowire ends. The combination of various fluorescence imaging techniques allows to get insight into the complexity of interactions between the up-converting nanocrystals and propagating plasmons in silver nanowires by determining factors contributing to the plasmonically enhanced up-conversion in rare-earths doped nanocrystals. They include energy transfer from NWs to NCs, radiative rate enhancement, and back energy transfer from NCs to NWs, which are the key findings of this work.

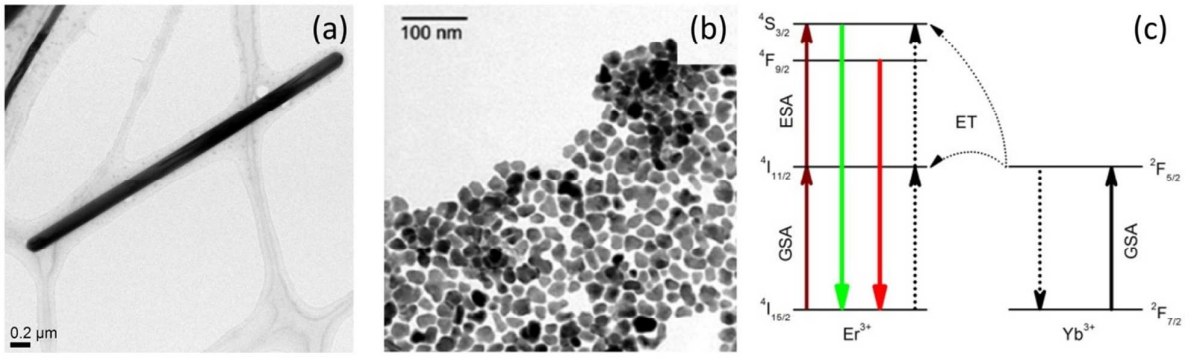

Figure 1. (a) A single silver nanowire observed using TEM. (b) $NaYF_4$:Er^{3+}/Yb^{3+} nanocrystals imaged using TEM. (c) Simplified energy diagram of up-conversion transitions observed in the Er^{3+}/Yb^{3+} system. Green and red lines represent $^4S_{3/2}\rightarrow{}^4I_{15/2}$ and $^4F_{9/2}\rightarrow{}^4I_{15/2}$ transitions in Er^{3+} ions, respectively.

2. Materials and methods

The hybrid nanostructure studied in this work consisted of silver nanowires deposited randomly on a glass substrate together with nanocrystals doped with Er^{3+}/Yb^{3+} ions. In contrast to organic dyes or semiconductor QDs, the emission of the up-converting NCs is extremely stable, it neither features blinking nor photobleaches under illumination. Furthermore, the infrared laser excitation generates essentially no background in the visible spectral range, enabling straightforward observation of photoluminescence. These unique properties of RE-doped up-converting nanocrystals renders them as excellent fluorophores for probing plasmonic interactions.

Silver NWs were synthesized by polyol process, as described elsewhere.[17] In Fig. 1a we show a transmission electron microscopy image of a single nanowire. On average the nanowires have diameters around 150 nm and lengths ranging from 1 to 10 µm. Due to the synthesis procedure, the NWs are covered with a 10-30 nm layer of PVP polymer. The polymer layer not only prevents silver oxidation, but also provides separation between nanowire and proximal fluorophores sufficient for inhibiting quenching of luminescence.[13] Extinction spectrum of Ag NW solution (Fig. 2S, supplementary) features broad band with a maximum at 400 nm and a tail extending towards 1000 nm. The broadening assures coupling with both absorption and emission of the nanocrystals. The colloidal $NaYF_4$:Er^{3+}/Yb^{3+} nanocrystals were synthesized as described previously.[30] The NCs form optically stable colloids in organic solvents with essentially no nanoparticle aggregation when deposited on a glass substrate. Transmission electron microscopy of these NCs show rather homogeneous particles with average diameter between 25 and 30 nm (Fig. 1b). When irradiated at 980 nm, the NCs exhibit green (550 nm) and red (660 nm) emission lines assigned to the $^4S_{3/2}\rightarrow{}^4I_{15/2}$ and $^4F_{9/2}\rightarrow{}^4I_{15/2}$ transitions in Er^{3+} ions,[31] respectively (Fig. 1c). This emission is a result of the up-conversion process in the Er^{3+}/Yb^{3+} system.[25] Hybrid nanostructures composed of $NaYF_4$:Er^{3+}/Yb^{3+} and silver nanowires were prepared by spin-coating 20 µl of the NC colloid on the substrate covered with randomly deposited silver nanowires. The concentration of both solutions allowed for obtaining substrates with well-separated Ag nanowires mixed with nanocrystals.

The optical properties of the hybrid NCs-NW system were examined using confocal fluorescence microscope equipped with dichroic mirror (2P 780 DC SPXR, Chroma) dedicated for the two-photon experiments. The sample was mounted on a piezoelectric scanning stage (P-517.3CL, Physik Instrumente) installed on top of the microscope body (Ti-S, Nikon). For excitation we used fiber coupled single mode laser diode (980 nm) operating in both continuous-wave (CW) and pulse modes (Spectra-Laser). The polarization of this laser is random at the fiber output. The sample was illuminated through an oil immersion objective (Plan Apo 60x NA=1.4, Nikon), which was also used for collecting luminescence signal. Typical laser power in front of the objective was about 5 mW CW. To visualize the distribution of silver nanowires on the substrate we raster-scanned the sample and detected the backscattered laser light using an APD detector (SPCM-16, PerkinElmer). The same detection channel equipped with appropriate band-pass filters (550/10 nm or 660/10 nm, Chroma) was used for photoluminescence imaging. Additionally, for polarization-sensitive experiments we mounted a linear polarizer (VIS-IR, colorPol) in the laser excitation path. The spatial resolution of the optical system was about 450 nm, limited by diffraction. Emission spectra were detected using a monochromator (Shamrock 500, Andor) coupled to a CCD camera (iDus, Andor). The spectral resolution was about 0.1 nm. Additionally, FLIM experiments were performed to probe the emission dynamics in the microsecond temporal range. To this end the APD was connected to a multiscaler card (MSA-300, Becker&Hickl) and triggered by a pulse generator (Keithley 3390). Luminescence transients were collected with 1 μs time resolution in a time window of 0-1 ms. Finally, for BFP imaging we used a CCD camera (iDus, Andor) and additional (Bertrand) lens.[32,33]

3. Results and discussion

3.1. Confocal and polarization-resolved microscopy

In Fig. 2 we summarize the results of confocal up-conversion luminescence imaging of a hybrid nanostructure composed of $NaYF_4:Er^{3+}/Yb^{3+}$ NCs and silver nanowires. All displayed maps were measured over the same sample area, as evidenced by identical positions of the silver nanowires. The elastic scattering image (Fig. 2a) features several randomly distributed silver nanowires with average length of around 5 μm. An up-conversion luminescence intensity map acquired for the detection wavelength of 660 nm, corresponding to red emission of Er^{3+}, features two qualitatively different subsets of emitters (Fig. 2b). First, we find round, isolated, and diffraction-limited spots with a size of about 450 nm and intensity of about 25000-30000 counts per second (cps) evenly distributed over the substrate. These values are comparable with previously reported,[34] indicating high up-conversion efficiency in the studied NCs. The luminescence spectrum obtained for such a single spot (Fig. 2c) is characteristic for Er^{3+} emission. Thus, we attribute these spots to the emission from individual or perhaps a few close lying $NaYF_4:Er^{3+}/Yb^{3+}$ NCs. As observed in the images shown in figure 2, some of the isolated spots are brighter than spots indistinguishably close to the nanowires. Therefore we conclude these brighter spots originate from aggregates of NCs, which our

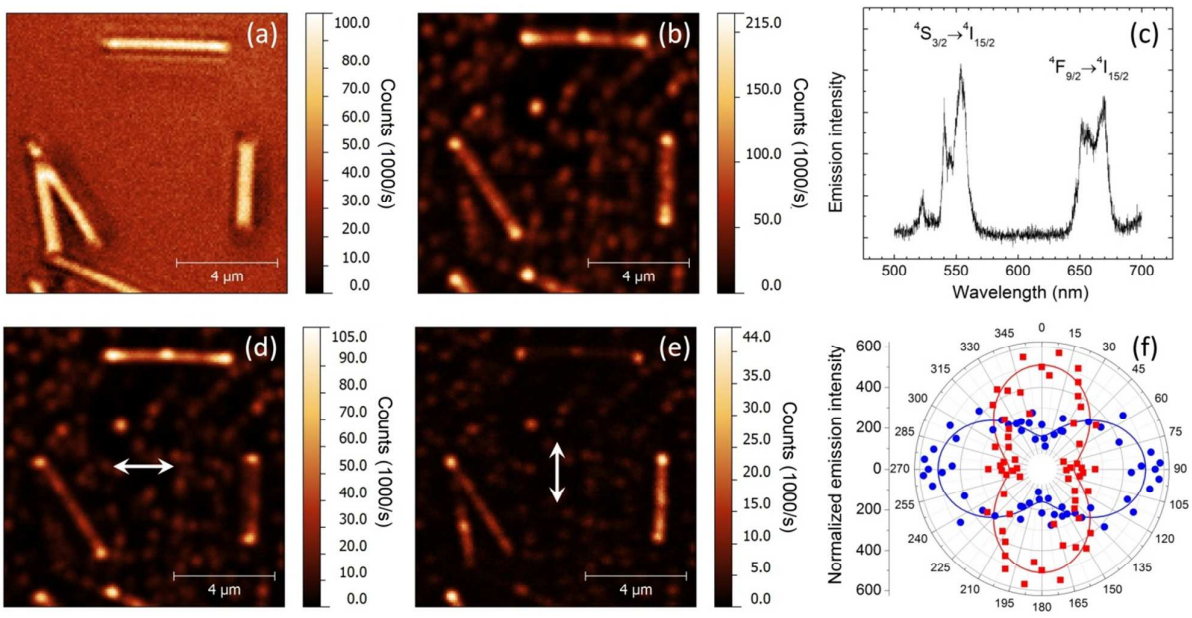

Figure 2. Summary of confocal imaging of hybrid nanostructures composed of silver nanowires and $NaYF_4:Er^{3+}/Yb^{3+}$ nanocrystals upon excitation at 980 nm. (a) Elastic scattering image visualizing the distribution of single nanowires on the glass. (b) Up-conversion luminescence intensity map acquired with 660 nm band-pass filter (unpolarised laser light) showing both individual, diffraction limited spots assigned to uncoupled nanocrystals as well as nanowires coupled with nanocrystals glowing with luminescence light. (c) Emission spectra taken from uncoupled NCs demonstrating Er^{3+} emission. Up-conversion fluorescence intensity maps acquired for vertically and horizontally polarized laser excitation are presented in figures (d) and (e), respectively. (f) Fluorescence intensity detected at 660 nm, integrated along nanowire hybrids and normalized by wire length plotted versus the nanowire's azimuthal orientation. Experimental points for vertical (●) and horizontal (■) polarization of the laser and fitted by sine squared and cosine squared functions.

experiments cannot distinguish from single NCs. We refer to those spots distinguishably removed from the NWs as 'uncoupled' NCs. The second subset comprises very bright stripes, whose length and position on the substrate correlates with the positions of the nanowires observed in the scattering image. The emission intensity in this case is approximately 7 times higher as compared to uncoupled nanocrystals, this enhancement is even stronger at the ends of the nanowires (Fig. 5S, supplementary). Comparable enhancement factors have been observed for similar plasmonic nanostructures, i.e. for silver nanowires coated with a very dense layer of nanocrystals also an enhancement factor of 7 was obtained.[10] Coupling up-converting nanocrystals with spherical Au nanoparticles resulted in slightly smaller values of enhancement (about 5-fold).[11] The largest, 14-fold, increase of emission intensity was achieved for $NaYF_4$:Yb,Er@SiO_2@Ag core-shell nanostructures.[12]

Since the NWs absorb in the infrared, the laser beam focused by the high NA objective launches SPPs that efficiently propagate along the nanowire.[9] The energy associated with the plasmons can be subsequently transferred to nearby nanocrystals or, to be more precise, to Er^{3+} and Yb^{3+} ions. This process can be directly visualized using polarization-resolved fluorescence microscopy. In Fig. 2d-e we show luminescence intensity maps detected at 660 nm for two orthogonal linear polarizations of the excitation laser. The detection was not polarization-selective. Three different cases can be observed in these images.

For a horizontal polarization of the laser the emission intensity is the strongest for a nanowire also aligned horizontally. At the same time, for orthogonally (vertically) oriented nanowire the luminescence intensity is dramatically diminished. The situation is precisely reversed for vertical polarization of the excitation laser. Finally, for nanowires tilted by 45° with respect to the polarization direction, the emission intensity shows little sensitivity to the polarization of the excitation. We note that for uncoupled nanocrystals we find no polarization-sensitive response, which we interpret is due to the absence of a preferred orientation of the transition dipole moment in these nanostructures.[33] We conclude that the polarization contrast of the $NaYF_4:Er^{3+}/Yb^{3+}$ nanocrystal luminescence is controlled by the nanowire.

In order to quantify the influence of the excitation polarization on the luminescence intensity, we analysed the emission of 30 individual nanowires. In Fig. 2f we display the integrated emission intensity along a nanowire plotted versus its azimuthal orientation. In order to compare the results obtained for nanowires with different lengths, we normalized the extracted intensities by the NW length and laser power for a given linear polarization. Experimental points marked as circles (blue) and squares (red) correspond to the intensities measured for vertical and horizontal laser polarization, respectively. We observe sine squared and cosine squared dependencies. Such a behaviour observed for linearly polarized light interacting with elongated nanostructures indicates that the interaction results in absorption enhancement in such a hybrid nanostructure. We attribute the observable intensity offset of about 150 cps to emission from uncoupled nanocrystals which are not polarization-sensitive. We conclude that that silver nanowires act as strongly polarization-sensitive optical nano-antennas which collect IR radiation by exciting propagating plasmons and transferring the excitation energy to nearby nanocrystals, opening thus an additional plasmon-mediated absorption channel.

3.2. Time-resolved microscopy

In the case of uncoupled $NaYF_4:Er^{3+}/Yb^{3+}$ nanocrystals, the infrared radiation is absorbed and converted by the Er^{3+}/Yb^{3+} system. However, nanocrystals placed in a close vicinity of the silver nanowires should experience modified local density of optical states (LDOS) which modulate theirs emission rates.[35] The key signature of spontaneous emission rate modifications due to interaction between an emitter and a metallic nanoparticle is the shortening of its luminescence lifetime.[2] We probed and spatially resolved the influence of plasmon coupling using fluorescence lifetime imaging microscopy. The detected transients could typically be described by a bi-exponential model function. Bi- or multiexponential decay behaviour could be expected due to the possibility of NC to NW energy transfer (ET) and unspecific interactions with surface ligands[36]. To analyse and visualize the recorded data we used an intensity-weighted average lifetime[2] $\bar{\tau} = (\alpha_1\tau_1^2 + \alpha_2\tau_2^2)/(\alpha_1\tau_1 + \alpha_2\tau_2)$, where $\tau_{1/2}$ are the luminescence decay times and $\alpha_{1/2}$ are the corresponding amplitudes at t=0.

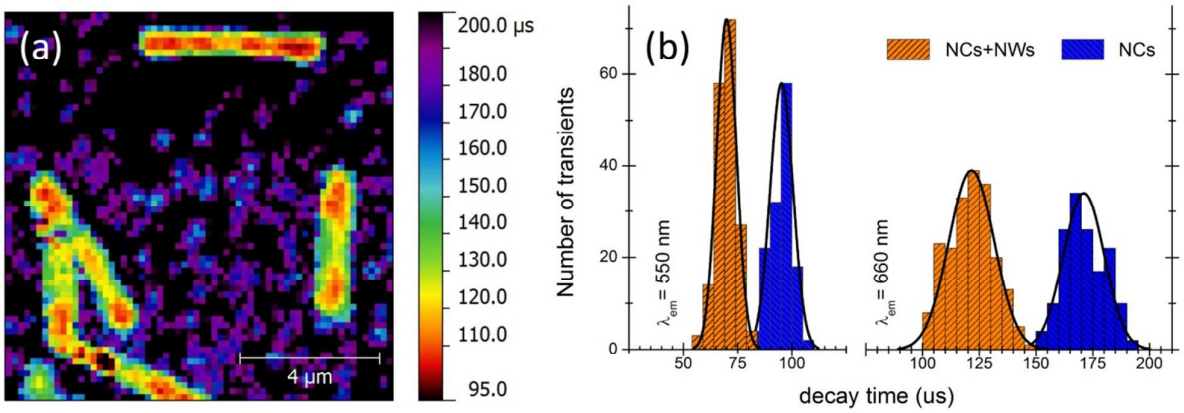

Figure 3. (a) The same area as in figure 2 visualized with FLIM at 660 nm, demonstrates shortening of decay time in the vicinity of silver nanowires. (b) Histograms of the average lifetimes for uncoupled (blue) and metal-coupled (orange) NaYF4:Er^{3+}/Yb^{3+} nanocrystals, collected for $^4S_{3/2}\rightarrow{}^4I_{15/2}$ (550 nm) and $^4F_{9/2}\rightarrow{}^4I_{15/2}$ (660 nm) transitions. The significant shift towards shorter lifetimes, from 90 µs to 70 µs for green and from 170 µs to 120 µs for red emission, proves efficient non-radiative coupling between NCs and silver NWs.

The spatial distribution of the average luminescence lifetimes recorded for the red emission of erbium ions at 660 nm is presented in Fig. 3a. For nanocrystals that are decoupled from the nanowires a typical average lifetime was about 170-180 µs. However, in the vicinity of the silver nanowires the dynamics changes, and the decay becomes substantially faster, with characteristic lifetimes ranging from 110 to 120 µs. This shortening of the decay time indicates strong radiative rate enhancement due to interaction between nanocrystals and metallic nanowires.[35] Particularly interesting is the fact that at the nanowire ends the luminescence dynamics is even faster, with characteristic lifetimes reaching 100 µs or less, as presented in Fig. 3a. We assign this to an increased coupling efficiency between NCs and particular NWs due to the broader range of available k vectors corresponding to an increased LDOS at the NWs ends. Strong enhancement of radiative transition rates at NWs ends manifests itself also as much brighter emission, as can be seen in Fig. 2b.

In order to get insight into statistically relevant data, we measured over a hundred of luminescence transients for uncoupled and metal-coupled nanocrystals for the green and red emission lines. The average lifetimes obtained for green and red emission are presented as histograms in Fig. 3b. For uncoupled NCs we find maxima at 90 and 170 µs for green and red emission, respectively, in accordance with previous studies of similar NCs.[37] In contrast, for NCs coupled to the NWs we observe a significant reduction of measured lifetimes, with maxima at 70 µs and 120 µs for green and red emission, respectively. This substantial shortening of the luminescence lifetime proves efficient interaction between silver NWs and emitting nanocrystals which enhances their emission rates. This effect, together with the increased absorption discussed above, contributes to the overall enhancement of the up-conversion luminescence.

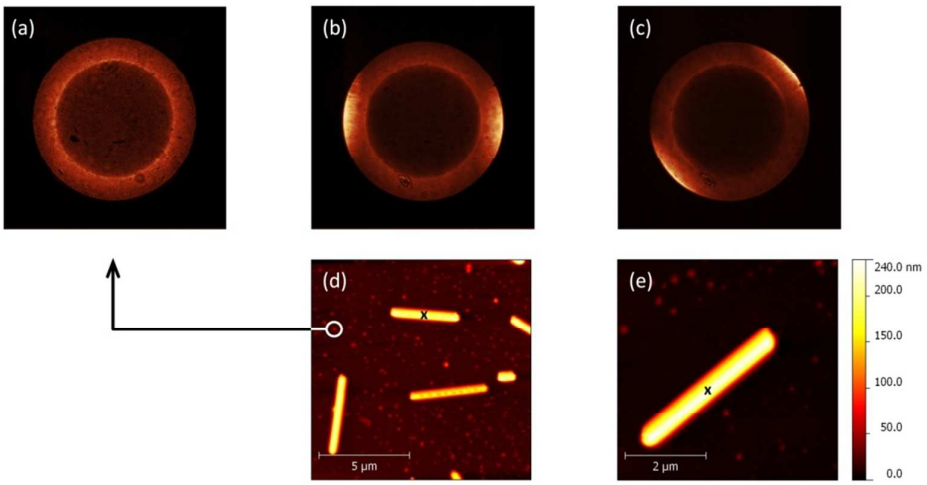

Figure 4. Back focal plane imaging of the hybrid systems excited upon 980 nm, detected at 660 nm. (a) Reference pattern recorded for an uncoupled $NaYF_4:Er^{3+}/Yb^{3+}$ nanocrystals. (b, c) Radiation patterns collected from hybrids excited at positions indicated by "X" in the AFM images shown below in (d) and (e).

3.3. Back Focal Plane microscopy

While time-resolved studies can be used to reveal new antenna-mediated relaxation channels as discussed above, they do not provide information on where the radiation is going and importantly, whether it is detected in the experiment. This facet of plasmon-mediated emission in coupled NCs-NW hybrids can be directly probed using back focal plane microscopy.[33,38] This technique allows to determine both the orientation of the dipolar emitters and the direction of plasmon propagation by analysing the angular distribution of emitted light in Fourier space.[39] The results displayed in Fig. 4a, where the pattern of the red emission of Er^{3+} from an uncoupled nanocrystals are monitored, shows a radially symmetric circular shape. Such pattern results from a superposition of hundreds of emitting dipoles (Er^{3+} ions) randomly positioned and oriented in a nanocrystal. On the other hand, radiation patterns collected from $NaYF_4:Er^{3+}/Yb^{3+}$ nanocrystals coupled to silver nanowires are qualitatively different (Fig. 4b-c). In addition to the rim characteristic for the uncoupled nanocrystals, two bright lobes can be easily recognized. The position of these lobes strictly follows the orientation of the nanowires. We conclude that up-converted luminescence energy upon being transferred from the nanocrystals to the nanowires, launches surface plasmons polaritons that propagate along the nanowire. This enhanced up-converted luminescence can be re-emitted as a leakage radiation, which results in the characteristic two lobe patterns.[33]

4. Conclusions

Using luminescence imaging we demonstrated very efficient coupling between up-converting $NaYF_4:Er^{3+}/Yb^{3+}$ nanocrystals and silver nanowires. In the vicinity of a single NW the up-conversion process is strongly enhanced, on average by a factor of 7. By combining time-resolved and polarization-resolved imaging we identified two processes, which contribute to this effect. While polarization-resolved microscopy indicates that silver NWs behave like receiving optical antennas, which efficiently collect IR radiation and

transfer the excitation energy directly to the NCs, FLIM microscopy proves the effect of plasmon excitations in silver nanowires on radiative transition rates of NCs placed in their vicinity. The energy flow after coupling to the nanowire was then visualized using back focal plane imaging. Characteristic double lobe patterns reflecting the orientation of the silver nanowires, confirms that excited NCs launch surface plasmons polaritons that are capable of efficient distribution of luminescence light within such a hybrid system. This observation can help to improve the design and understanding of plasmonic networks employing silver nanowires as nano-guides for luminescence energy.

Acknowledgements

Financial support by the ERC through the starting grant NEWNANOSPEC, the Deutsche Forschungsgemeinschaft (DFG) through the Nanosystems Initiative Munich (NIM), the Polish National Science Centre through projects N N202 238940 and DEC-2013/09/D/ST3/03746, Foundation for Polish Science through WELCOME project “Hybrid Nanostructures as a Stepping Stone towards Efficient Artificial Photosynthesis” and the Polish Ministry of Science and Higher Education through Mobility Plus project (633/MOB/2011/0) is gratefully acknowledged.

References

1. E. M. Purcell, *Phys. Rev.*, **69**, 681.
2. J. R. Lakowicz, *Principles of Fluorescence Spectroscopy*, Springer, 3rd edn., 2006.
3. C. Höppener and L. Novotny, *Q. Rev. Biophys.*, 2012, **45**, 209–255.
4. Q.-C. Sun, H. Mundoor, J. C. Ribot, V. Singh, I. I. Smalyukh and P. Nagpal, *Nano Lett.*, 2013.
5. D. G. Zhang, X.-C. Yuan, A. Bouhelier, P. Wang and H. Ming, *Opt. Lett.*, 2010, **35**, 408–410.
6. S. Mackowski, *J. Phys. Condens. Matter*, 2010, **22**, 193102.
7. Y. Fu, J. Zhang and J. R. Lakowicz, *Biochem. Biophys. Res. Commun.*, 2008, **376**, 712–717.
8. K. Okamoto, S. Vyawahare and A. Scherer, *J. Opt. Soc. Am. B*, 2006, **23**, 1674–1678.
9. H. Wei, D. Ratchford, X. (Elaine) Li, H. Xu and C.-K. Shih, *Nano Lett.*, 2009, **9**, 4168–4171.
10. W. Feng, L.-D. Sun and C.-H. Yan, *Chem. Commun.*, 2009, 4393–4395.
11. S. Schietinger, T. Aichele, H.-Q. Wang, T. Nann and O. Benson, *Nano Lett.*, 2010, **10**, 134–138.
12. P. Yuan, Y. H. Lee, M. K. Gnanasammandhan, Z. Guan, Y. Zhang and Q.-H. Xu, *Nanoscale*, 2012, **4**, 5132–5137.
13. P. Bharadwaj and L. Novotny, *Opt. Express*, 2007, **15**, 14266–14274.
14. V. Biju, *Chem. Soc. Rev.*, 2013.
15. G. Walters and I. P. Parkin, *J. Mater. Chem.*, 2009, **19**, 574–590.
16. Y. Xia, *SPIE Newsroom*, 2008.
17. M. Olejnik, B. Krajnik, D. Kowalska, M. Twardowska, N. Czechowski, E. Hofmann and S. Mackowski, *Appl. Phys. Lett.*, 2013, **102**, 083703.
18. B. Wild, L. Cao, Y. Sun, B. P. Khanal, E. R. Zubarev, S. K. Gray, N. F. Scherer and M. Pelton, *ACS Nano*, 2012, **6**, 472–482.
19. A. V. Akimov, A. Mukherjee, C. L. Yu, D. E. Chang, A. S. Zibrov, P. R. Hemmer, H. Park and M. D. Lukin, *Nature*, 2007, **450**, 402–406.
20. C. Gruber, P. Kusar, A. Hohenau and J. R. Krenn, *Appl. Phys. Lett.*, 2012, **100**, 231102.
21. A. Paul, D. Solis, K. Bao, W.-S. Chang, S. Nauert, L. Vidgerman, E. R. Zubarev, P. Nordlander and S. Link, *ACS Nano*, 2012, **6**, 8105–8113.
22. C. Gruber, A. Trügler, A. Hohenau, U. Hohenester and J. R. Krenn, *Nano Lett.*, 2013, **13**, 4257–4262.
23. H. Wei, Z. Li, X. Tian, Z. Wang, F. Cong, N. Liu, S. Zhang, P. Nordlander, N. J. Halas and H. Xu, *Nano Lett.*, 2011, **11**, 471–475.
24. G. Blasse and B. C. Grabmaier, *Luminescent materials*, Springer-Verlag, 1994.
25. F. Auzel, *Chem. Rev.*, 2004, **104**, 139–174.
26. R. Kumar, M. Nyk, T. Y. Ohulchanskyy, C. A. Flask and P. N. Prasad, *Adv. Funct. Mater.*, 2009, **19**, 853–859.
27. Q. Liu, Y. Sun, C. Li, J. Zhou, C. Li, T. Yang, X. Zhang, T. Yi, D. Wu and F. Li, *ACS Nano*, 2011, **5**, 3146–3157.
28. W. G. van Sark, J. de Wild, J. K. Rath, A. Meijerink and R. E. Schropp, *Nanoscale Res. Lett.*, 2013, **8**, 1–10.
29. B. Henke, *SPIE Newsroom*, 2009.
30. M. Nyk, R. Kumar, T. Y. Ohulchanskyy, E. J. Bergey and P. N. Prasad, *Nano Lett.*, 2008, **8**, 3834–3838.
31. D. Piatkowski and S. Mackowski, *Opt. Mater.*, 2012, **34**, 2055–2060.
32. N. Hartmann, G. Piredda, J. Berthelot, G. Colas des Francs, A. Bouhelier and A. Hartschuh, *Nano Lett.*, 2012, **12**, 177–181.
33. N. Hartmann, D. Piatkowski, R. Ciesielski, S. Mackowski and A. Hartschuh, *ACS Nano*, 2013, **7**, 10257–10262.
34. A. D. Ostrowski, E. M. Chan, D. J. Gargas, E. M. Katz, G. Han, P. J. Schuck, D. J. Milliron and B. E. Cohen, *ACS Nano*, 2012, **6**, 2686–2692.
35. W. Barnes, *J. Mod. Opt.*, 1998, **45**, 661–699.
36. F. Wang, J. Wang and X. Liu, *Angew. Chem. Int. Ed.*, 2010, **49**, 7456–7460.
37. J. Zhao, Z. Lu, Y. Yin, C. McRae, J. A. Piper, J. M. Dawes, D. Jin and E. M. Goldys, *Nanoscale*, 2013, **5**, 944.
38. T. Shegai, V. D. Miljković, K. Bao, H. Xu, P. Nordlander, P. Johansson and M. Käll, *Nano Lett.*, 2011, **11**, 706–711.
39. M. A. Lieb, J. M. Zavislan and L. Novotny, *J. Opt. Soc. Am. B*, 2004, **21**, 1210–1215.